High-resolution adaptive phase distortion compensation using a diffractive-feedback system: experimental results

Mikhail A. Vorontsov

U.S. Army Research Laboratory, Information Science and Technology Directorate, Adelphi, Maryland 20783

Received February 8, 1999; revised manuscript received May 5, 1999; accepted May 20, 1999

An adaptive system having 70,400 wave-front control channels has been experimentally analyzed. Wave-front control is based on the diffractive-feedback principle and requires neither a reference wave nor direct wave-front measurements. The key system elements are a liquid-crystal television used as a phase modulator, a CCD camera, and an optoelectronic feedback loop. Experiments demonstrated efficient suppression of wave-front distortions belonging to a bandpass spectral domain. Results demonstrate the system's potential as a secondary high-resolution adaptive feedback system for adaptive optics applications. © 1999 Optical Society of America [S0740-3232(99)01510-0]

OCIS codes: 010.0010, 100.5070, 060.5060, 070.6020, 050.1970.

1. INTRODUCTION

Wave-front distortions that are small in comparison with an optical system's aperture size may significantly limit the performance of a variety of optical systems: Atmospheric imaging systems, laser communication systems, optical processing systems, and industrial laser systems are only a few on the list. The compensation of small-scale phase distortions (phase noise) is in some sense a more difficult task than the suppression of light intensity fluctuations (intensity noise), which can be performed by using a conventional Fourier filtering technique.[1] The system described here is designed to provide high-resolution bandpass phase distortion compensation (filtering). This phase noise filtering occurs without direct phase distortion measurements and does not suffer from significant energy losses.

Small-scale phase distortions can potentially be suppressed by using known techniques such as nonlinear optical phase conjugation,[2] dynamical holography,[3] or adaptive optics.[4] All of these techniques have various drawbacks that limit their practical application. Phase conjugation typically requires that the source of the phase distortions be located in the optical path of both the outgoing and reflected waves. The disadvantages of dynamical holography are the relatively low diffractive efficiency and the necessity to have an undistorted reference wave. A reference wave is also required for the more recently developed high-resolution all-optical adaptive systems based on direct use of an interference pattern for control of an optically addressed phase spatial light modulator (phase SLM).[3,5–7] Conventional adaptive optics techniques based on direct wave-front measurements and the use of controllable mirrors or liquid-crystal (LC) phase modulators are effective only for the compensation of large-scale phase distortions. The transition to high-resolution adaptive wave-front control (more than 10^3 control channels) would lead to an unacceptable increase in system cost, size, and complexity primarily because of the technical difficulties in high-resolution wave-front reconstruction.

Recently, new algorithms for high-resolution wave-front control that do not require either a reference wave or direct wave-front measurements—adaptive systems with diffractive feedback—have been proposed.[8–10] With the diffractive-feedback approach, wave-front phase distortion correction is performed by using the intensity distribution of a wave that passes through a high-resolution wave-front corrector and then diffracts a short distance in the system's feedback loop. Diffraction of this phase-modulated wave provides for transformation of the residual wave-front phase distortion into its corresponding intensity distribution, which can be directly used to control the input wave phase.

Here the first experimental implementation of a diffractive-feedback adaptive system is reported, and its potential is demonstrated for small-scale phase distortion suppression. The phase modulator used in the experiments is a twisted nematic liquid-crystal television (LCTV) panel from the Epson Crystal Image video projector operated in the phase modulation regime. The number of control channels N in the adaptive system is equal to the number of LCTV panel pixels ($N = 220 \times 320 = 70{,}400$). Wave-front correction is achieved by using iterative control algorithms similar to those described in Ref. 10. This work is different from previous experiments with LCTV panel-based adaptive systems that used a registered interference pattern as the feedback signal.[11–13]

2. ADAPTIVE SYSTEM WITH DIFFRACTIVE FEEDBACK: EXPERIMENTAL SETUP

A schematic of the experimental setup is shown in Fig. 1. The argon laser beam ($\lambda = 0.514$ μm) was expanded to

0740-3232/99/102567-07$15.00

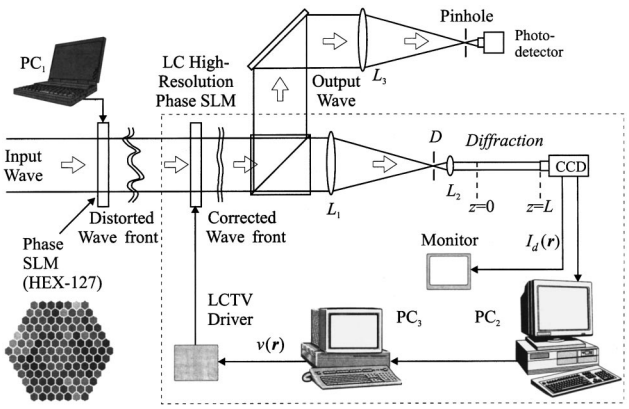

Fig. 1. Schematic of the adaptive system used in the experiments. The focal lengths corresponding to lenses L_1, L_2, and L_3 are $f_1 = 1000$ mm, $f_2 = 125$ mm, and $f_3 = 350$ mm.

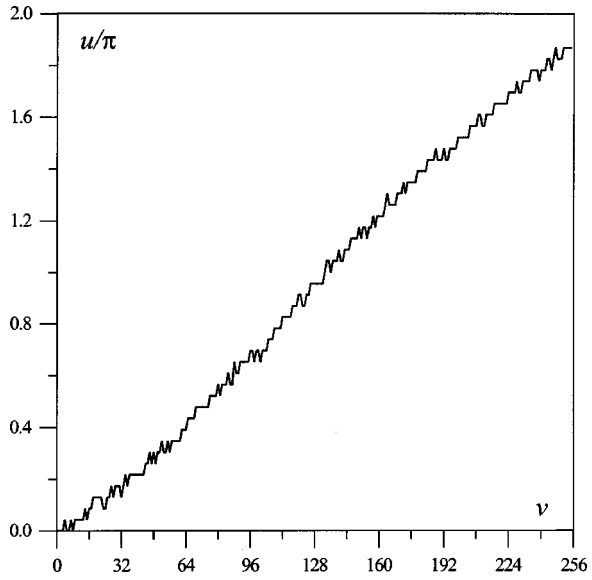

Fig. 2. Phase-modulation characteristic of the LCTV.

a diameter of 30 nm and then passed through a multielement LC HEX127 phase modulator from Meadowlark Optics, Inc. The LC modulator was used to introduce piston-type phase distortions $\phi(\mathbf{r})$ [$\mathbf{r} = \{x, y\}$ is a vector in the transverse plane]. The phase modulator has 127 hexagon-shaped LC cells controlled by a personal computer (PC_1). Each cell is 1.15 mm in diameter with 36-μm spacing. The LC cell geometry is shown in Fig. 1 at the bottom left.

The distorted wave is incident on the adaptive system shown inside the dashed box in Fig. 1. The adaptive system consists of a LCTV panel (LC phase SLM with clear aperture 20×26 mm), two lenses (L_1 and L_2), a CCD camera, an EPIX image processing system based on a personal computer (PC_2), and a third computer (PC_3) that controls the LCTV panel electronic driver. The LCTV panel introduces an additional phase modulation $u(\mathbf{r})$ that attempts to compensate wave-front distortions in the input wave. The depth of the introduced phase modulation is dependent on the controlling signal $v(\mathbf{r})$, which is measured in video signal gray levels. The controlling signal $v(\mathbf{r})$ was formed through digital processing of the intensity distribution $I_d(\mathbf{r})$ as registered by the CCD camera and then sent to the driver controlling the LCTV panel. The LCTV driver was adjusted so that the phase modulation characteristic $u = F(v)$ was close to linear, as shown in Fig. 2. The image $v(\mathbf{r})$ was displayed on the monitor of PC_3. As seen in Fig. 2, the wave-front correction dynamical range for the LCTV panel was on the order of 2π rad. Note that the LCTV panel itself introduced large-scale parasitic phase and intensity modulations with a peak-to-valley value on the order of 10% of the entire dynamical range.

The LCTV panel was located in the front focal plane of lens L_1 (Fig. 1). Diaphragm D was placed in the common focal plane of lenses L_1 and L_2 and used as a low-pass spatial filter. With a fully opened diaphragm, the lens system decreased the input beam size by a factor of $M = 8$ in the rear focal plane of L_2 ($z = 0$). Diffraction of the phase-modulated wave occurred between the plane $z = 0$ and the plane of the CCD camera imaging chip ($z = L$). The CCD camera (Panasonic CCTV) has 771×492 pixels within an active area of 4.82×3.64 mm. The input beam size was decreased for two reasons: (1) to provide an approximate match between the LCTV and CCD active area sizes (an additional image scaling was performed digitally) and (2) to decrease the required diffractive distance L by a factor of M^2.[10] In the experiments the wave diffraction length L was on the order of 4–10 nm.

The registered intensity $I_d(\mathbf{r})$ was displaced on the TV monitor and digitized. The controlling image $v(\mathbf{r})$ was calculated based solely on the intensity distribution $I_d(\mathbf{r})$. Wave-front correction efficiency was then analyzed by using the output beam spatial spectrum obtained by the Fourier lens L_3. Measurements of the laser beam energy P inside a pinhole of size 50 μm located in the focal plane of lens L_3 were used to calculate the Strehl ratio $\mathrm{St} = P/P_0$, where P_0 is the laser beam energy corresponding to the undistorted input wave.

3. WAVE-FRONT CONTROL: ALGORITHMS AND SIGNAL PROCESSING

Control algorithms for phase distortion correction based on the diffractive-feedback approach were analyzed in Ref. 10. A control algorithm defines dependence of a phase modulation function $u(\mathbf{r},t)$ on the measured information [diffractive $I_d(\mathbf{r}, t)$ and input $I_{\mathrm{in}}(\mathbf{r})$ intensity distributions]. In the case of diffractive feedback, this dependence can be expressed in the form of a nonlinear differential (integro-differential) or iterative equation describing control system dynamics. Stationary-state solution of the control equation should correspond to wave-front correction and result in the spatially uniform residual phase $\delta(\mathbf{r}, t) = u(\mathbf{r}, t) + \phi(\mathbf{r})$: $\delta(\mathbf{r}, t) \to$ constant for $t \to \infty$. Represent the control algorithm in the form of a continuous dynamical process[10]:

$$\tau \frac{\mathrm{d}u(\mathbf{r}, t)}{\mathrm{d}t} + u = K w_{\mathrm{FB}}(\mathbf{r}, t), \qquad (1)$$

$$w_{\mathrm{FB}}(\mathbf{r}, t) = \int h(\mathbf{r} - \mathbf{r}')F[I_d(\mathbf{r}', t), I_{\mathrm{in}}(\mathbf{r}')]\mathrm{d}^2\mathbf{r}'. \quad (2)$$

Here $u(\mathbf{r}, t)$ is the introduced phase modulation, τ is the system time response, and K is the feedback gain coefficient. The convolution integral in Eq. (2) describes spatial filtering applied to function F. The spatial filter response function $h(\mathbf{r})$ is the Fourier transform of the spatial filter transfer function $H(\mathbf{q})$, where $\mathbf{q}$ is the spatial frequency. Spatial filtering is required to prevent control system instability. Phase distortion compensation can be achieved by using various functions for F and $h(\mathbf{r})$. In the simplest case, Kerr-slice/feedback mirror-type dynamics,[8,9] the function F is dependent solely on the measured diffractive intensity distribution: $F(\mathbf{r}, t) = I_d(\mathbf{r}, t)$. For this case, instead of Eq. (2), we have

$$w_{\mathrm{FB}}(\mathbf{r}, t) = \int h(\mathbf{r} - \mathbf{r}')I_d(\mathbf{r}', t)\mathrm{d}^2\mathbf{r}'. \quad (3)$$

In the experiments the following modified discrete version of algorithm (1) and (3) was used:

$$u_{i,j}^{(n+1)} = (1 - \alpha)u_{i,j}^{(n)} + Kw_{i,j}^{(n)},$$

$$w_{i,j}^{(n)} = I_{i,j}^{(n)} * h_{i,j} \quad (i = 1,\ldots, N_x, \quad j = 1,\ldots, N_y), \quad (4)$$

where α and K are coefficients, $u_{i,j}^{(n+1)}$ is an image array of size $N_x \times N_y$ (320×220) at the $(n + 1)$th adaptation process iteration, and $I_{i,j}^{(n)}$ is an array corresponding to the registered intensity distribution $I_d(\mathbf{r}, t_n)$ after scaling. The notation $I_{i,j}^{(n)} * h_{i,j}$ stands for the discrete convolution of $I_{i,j}^{(n)}$ with a filtering function $h_{i,j}$. To keep phase modulation in the operational range (0–255 gray levels), the controlling image $v_{i,j}^{(n+1)}$ driving the LC phase SLM was obtained by subtracting the aperture-averaged value $\bar{u}^{(n+1)} = (N_x N_y)^{-1}\Sigma_{i,j}u_{i,j}^{(n+1)}$:

$$v_{i,j}^{(n+1)} = u_{i,j}^{(n+1)} - \bar{u}^{(n+1)} + \mathrm{const}. \quad (5)$$

The constant in Eq. (5) was added to have an averaged phase modulation in the middle of the modulation characteristic of the LCTV panel.

Along with digital filtering, we also used a low-pass optical Fourier filter. In this case the control algorithm can be simplified:

$$u_{i,j}^{(n+1)} = (1 - \alpha)u_{i,j}^{(n)} + K\tilde{I}_{i,j}^{(n)},$$

$$v_{i,j}^{(n+1)} = u_{i,j}^{(n+1)} - \bar{u}^{(n+1)} + \mathrm{const}$$

$$(i = 1,\ldots, N_x, \quad j = 1,\ldots, N_y), \quad (6)$$

where $\tilde{I}_{i,j}^{(n)}$ is an array corresponding to the intensity distribution $I_d(\mathbf{r}, t_n)$ in the system with low-pass optical spatial filter. In the experiments spatial filtering was performed by using the diaphragm D in Fig. 1. Replacing digital filtering by optical filtering simplifies the control algorithm, resulting in faster convergence.

An important factor for the adaptive system's performance is the input wave intensity modulation. In adaptive systems based on the diffractive-feedback principle, input beam intensity modulation may cause the appearance of an additional phase distortion.[9,10] To decrease the influence of the input field intensity modulation $I_{\mathrm{in}}(\mathbf{r})$, the control algorithm (4) and (5) was modified by introducing the spatially modulated gain coefficient $K(\mathbf{r})$:

$$K_{i,j} = K[2 - I_{i,j}^{\mathrm{ref}}/\max(I_{i,j}^{\mathrm{ref}})], \quad (7)$$

where $I_{i,j}^{\mathrm{ref}}$ is an array corresponding to the diffractive intensity distribution measured in the absence of phase distortions (reference intensity).

4. SPATIAL SPECTRAL BAND FOR PHASE DISTORTION COMPENSATION

An adaptive system with diffractive feedback can compensate phase distortions belonging to a limited spectral band $[q_A, q_B]$. This spectral band is dependent on the system's spatial filter cutoff frequency q_{cut} and the diffractive length L.[9,10] Consider the principal requirements for the parameters q_{cut} and L. In the absence of spatial filtering, the feedback system is unstable if the gain coefficient exceeds a threshold value of $|K| > |K_{\mathrm{th}}|$. Spatiotemporal instability occurs within the spectral range $q > q_1$, where $q_1 = 2\pi(\lambda L)^{-1/2}$.[8,9] The spatial filter cutoff frequency q_{cut} and the adaptive system operational spectral band $[q_A, q_B]$ can be determined based on stability analysis of the system.

For a simple low-pass spatial filter with cutoff frequency $q_{\mathrm{cut}} = q_1$, spatial frequencies q_A and q_B are derived in Appendix A: $q_A = [\pi^{-1}\arcsin(0.5|K|^{-1})]^{1/2}q_1$ and $q_B = q_1 - q_A$. Knowledge of q_A and q_B allows estimation of the range of phase distortion spatial scales $r_s < l < r_l$ that the adaptive system is capable of compensating. For an adaptive system with beam size demagnification in the feedback loop, $r_l = 2\pi M/q_A$ and $r_s = 2\pi M/q_B$. Using this approximation $\arcsin(0.5|K|^{-1}) \cong 0.5|K|^{-1}$ valid for $|K| \gg 1$, we can simplify these formulas: $q_A \cong [2\pi/(\lambda L|K|)]^{1/2}$, $r_l \cong M(2\pi\lambda L|K|)^{1/2}$, and $r_s \cong M(\lambda L)^{1/2}$. When the gain coefficient $|K|$ is increased, the width of the spectral band $[q_A, q_B]$ increases. In the adaptive system described here, the gain coefficient $|K|$ was on the order of 4–8 ($|K_{\mathrm{th}}| = 0.5$). For a characteristic diffractive distance $L = 4$ mm, gain coefficient $|K| = 4$, and magnification $M = 8$, we obtain $q_1 \cong 1380\ \mathrm{cm}^{-1}$ and $q_A \cong 0.2q_1$. The corresponding phase distortion spatial scales are $r_l \cong 1.8$ mm and $r_s \cong 0.45$ mm. Thus the adaptive system was able to compensate phase distortions having spatial scales l in the range $0.45\ \mathrm{mm} < l < 1.8$ mm.

To increase the adaptive system's operational range, we must decrease the diffractive length and increase the gain coefficient. The ability to decrease L to less than 4 mm is limited by the resolution of the phase modulator (pixel size of the LCTV). Increasing $|K|$ increases the undesired influence of input beam intensity nonuniformities on phase distortion compensation efficiency. For $|K| > 8$ additional phase distortions appeared, resulting from nonuniformities in the input beam intensity.

5. PHASE DISTORTION COMPENSATION: EXPERIMENTAL RESULTS

The results of adaptive system operation are shown in Figs. 3–6. Phase distortions were introduced into the in-

put laser beam by applying random voltages $\{g_m\}$ ($m = 1,\ldots, 127$) to the HEX127 phase modulator elements. The random values $\{g_m\}$ had a uniform probability distribution in the interval $[-g + g_0, g + g_0]$, where g_0 is the dc component and g is the amplitude. The value g_0 was added to operate in the linear region of the HEX127 modulation characteristic. The applied voltages caused random piston-type input wave phase shifts $\phi_m : \{-\phi + \phi_0 \leqslant \phi_m \leqslant \phi + \phi_0\}$, resulting in wave-front distortion. The wave-front distortion peak-to-valley amplitude is 2ϕ. This amplitude was controlled by the voltage amplitude g.

Consider first results of the adaptation process in a system with a low-pass optical filter (diaphragm D in Fig. 1), shown in Fig. 3. Wave-front correction was based on iterative procedure (6) with α=0.4, $K = -4$, and $L = 4$ mm. The amplitude of the random phase distortions ϕ was 0.6π rad. Phase distortion compensation efficiency can be examined by using diffractive intensity distributions $I_d(\mathbf{r}, t_n)$ registered during the adaptation process.

The intensity $I_d(\mathbf{r}, t_n)$ for the first three iterations is shown in Figs. 3(a)–3(c). The introduced random phase distortion resulted in a highly nonuniform initial diffractive intensity pattern $I_d(\mathbf{r}, t_n)$ ($n = 0$), as seen in Fig. 3(a). Wave-front correction suppressed most of the intensity modulation high-spatial-frequency components, as shown in the intensity pattern $I_d(\mathbf{r}, t_n)$ ($n = 3$) in Fig. 3(c). The controlling LCTV panel image $v(\mathbf{r}, t_3)$ is shown in Fig. 3(d). The wave-front correction in Fig. 3 caused the Strehl ratio to increase from 0.6 to 0.78. Typically, a stationary-state diffractive intensity pattern was achieved after 3–4 iterations, with an iteration rate of approximately 2 s per iteration.

As discussed in Section 4, the adaptive system with diffractive feedback provides only bandpass-type phase distortion compensation. Furthermore, adaptation may result in the appearance of additional large-scale phase distortions. The origin of these phase distortions is large-scale nonuniformities present in the input/diffractive intensity distribution [see, for example, the stripes in Fig. 3(c)]. Because of the controlling signal's dependence on the diffractive intensity, these nonuniformities are transformed into a corresponding modulation of the controlling image and phase [see the stripes in the controlling image in Fig. 3(d)]. This induced large-scale phase modulation cannot be compensated by the adaptive system itself.

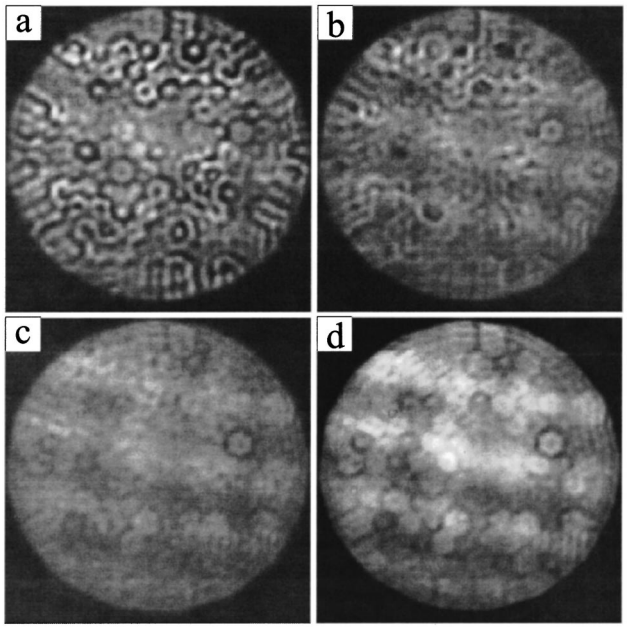

Fig. 3. Experimental results of phase distortion compensation in a system with optical filtering: diffractive intensity registered by the CCD camera (a) without adaptation (b) after the first iteration, (c) after the first three iterations; (d) is the controlling gray-scale pattern corresponding to (c).

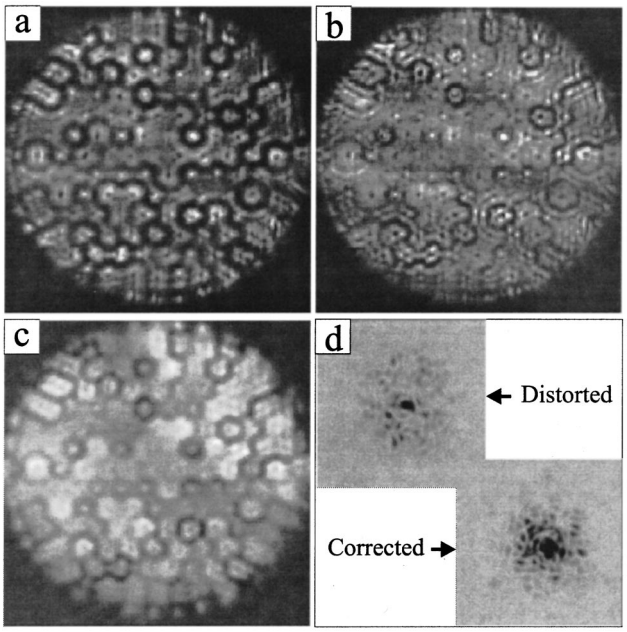

Fig. 4. Compenstion of phase distortions by using a control algorithm with spatially modulated gain and digital filtering: (a) and (b) are diffractive intensity patterns [(a) without adaptation and (b) after five iterations], (c) is the controlling gray-scale pattern corresponding to (b), and (d) shows spatial spectra corresponding to distorted (top) and corrected (bottom) output waves. Wave-front correction was based on iterative procedure (4), (5), and (7) with α=0.4, $K = -4$, and $L = 4$ mm.

The impact of input field intensity modulation can be decreased by using the control algorithm with spatially modulated gain coefficient (7) described in Section 3. Figure 4 presents results of adaptation obtained by using control algorithm (4) with the spatially modulated gain coefficient (7). The spatial filtering in algorithm (4) is performed digitally, and thus the optical spatial filter was removed. The introduced phase distortion amplitude was $\phi = 3\pi$ rad. The initial diffractive intensity modulation caused by the phase distortion seen in Fig. 4(a) was largely compensated in the stationary-state intensity pattern in Fig. 4(b). The remaining large- and small-scale intensity modulation seen in Fig. 4(b) indicates the presence of residual phase distortions that do not belong to the system operational band. Note that the stripe-type large-scale modulation seen in the images in Figs. 3(d) and 4(b) is barely present in the controlling image in Fig. 4(c). This demonstrates that using a spatially modulated gain coefficient can reduce the influence of input beam intensity modulation.

Spatial spectra for both distorted and corrected waves are shown in Fig. 4(d). To show the redistribution of the energy in the spatial spectra caused by adaptation, both images in Fig. 4(d) are normalized by the corresponding maximum intensities. Adaptation narrowed the spatial spectrum and increased the amplitude of the zero spectral component. As a result of bandpass phase distortion compensation, the Strehl ratio increased from 0.25 to 0.45.

Diffractive-feedback system efficiency for compensating "natural" small-scale phase distortions was analyzed by using a piece of Plexiglas placed in front of the HEX127 phase modulator shown in Fig. 1. This standard Plexiglas plate has a nonuniform thickness related to the manufacturing process. The thickness variation caused phase distortions having a characteristic spatial scale on the order of 0.3–1.0 mm and a characteristic phase distortion amplitude ranging from 0.2π to 1.0π. The Strehl ratio correspondingly decreased from 0.5 to approximately 0.25. The adaptive system was able to increase the Strehl ratio up to 0.45. As shown in Figs. 5(a) and 5(b), patterns for the diffractive intensity distributions obtained before and after adaptation demonstrate efficient suppression of the Plexiglas-induced phase distortions.

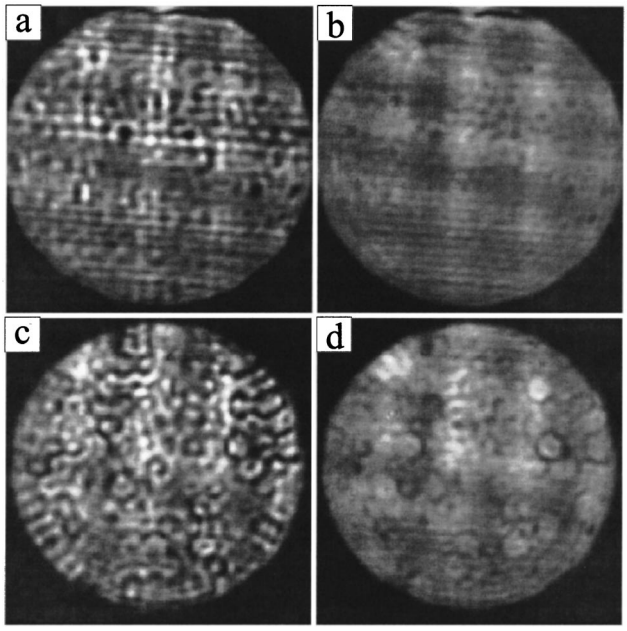

Fig. 5. Adaptive compensation of phase distortions introduced into the input beam by using (a), (b) Plexiglas plate and (c), (d) both the Plexiglas plate and the HEX127 phase modulator; (a) and (c) are the diffractive intensity patterns without adaptation, and (b) and (d) are those with adaptation. Wave-front correction was based on iterative procedure (6) with $\alpha = 0.3$, $K = -4$, and $L = 4$ mm.

Table 1. Diffractive-Feedback System Phase Distortion Compensation Efficiency

Aberration Amplitude ϕ (rad)	$\langle S_t \rangle$ without Adaptation	$\langle S_t \rangle$ with Adaptation	
		$L = 4$ mm, $K = 4$	$L = 8$ mm, $K = 8$
1.8 (HEX127)	0.60	0.78	0.78
4.4 (HEX127)	0.35	0.56	0.65
6.9 (HEX127)	0.28	0.48	0.57
Plexiglas	0.30	0.40	0.50
8.9 (HEX127 and Plexiglas)	0.15	0.25	0.40

Multiscale phase distortion compensation is demonstrated in Figs. 5(c) and 5(d). Here both the Plexiglas plate and the HEX127 phase modulator were used to create phase distortions. The amplitude of random phase aberration introduced by the HEX127 modulator was $\phi = 2\pi$ rad. The adaptive system was able to increase the Strehl ratio by a factor of 1.5.

To increase the spatial width of the phase distortion compensation band, values of both the diffractive length L and the gain coefficient $|K|$ were increased by a factor of 2 ($L = 8$ mm and $|K| = 8$). For these parameter values, the adaptive system operational band was 0.5 mm $< l <$ 3.6 mm (for $L = 4$ mm and $|K| = 4$, 0.45 mm $< l <$ 1.8 mm).

Results of adaptation for various random phase distortion amplitudes ϕ are given in Table 1. Values of the Strehl ratio $\langle St \rangle$ were obtained by averaging over ten realizations of the applied random phase aberrations. Strehl ratio measurements were performed after five wave-front correction iterations using iterative control algorithm (4) and (7). The results in Table 1 show that extending the adaptation spatial band improved adaptive system efficiency.

6. SPATIOTEMPORAL INSTABILITIES

Increasing the feedback gain coefficient $|K|$ beyond a certain value can result in the appearance of different types of spatiotemporal instabilities. Wavetype instabilities as shown in Fig. 6(a) were observed in the presence of strong (4–6-wavelength) large-scale phase distortions (tilts, defocus, astigmatisms, etc.). The traveling-shock-wave-type instabilities seen in Fig. 6(b) occurred when the value for the coefficient α in algorithms (4) and (6) were set near unity. The case $\alpha = 1$ corresponds to a control algorithm without memory: Phase modulation is completely updated at each iteration step. For $\alpha > 0.6$ and $|K| > 10$, the adaptation process was unstable in most cases. For this reason the parameter α used in the experiments was on the order of 0.1–0.5. Decreasing α slowed adaptation process convergence.

Spatiotemporal instabilities in the form of transverse patterns arose in the diffractive-feedback system when the spatial filter bandwidth was increased. The self-organized square and hexagon-type patterns shown in Figs. 6(c) and 6(d) were obtained with the use of the Gaussian-type spatial filter with characteristic bandwidth $q_{cut} > q_1$.

7. CONCLUDING REMARKS

An adaptive system having 70,400 control channels has been experimentally demonstrated. Wave-front control is based on the intensity distribution of a wave that propagates a short distance between the wave-front cor-

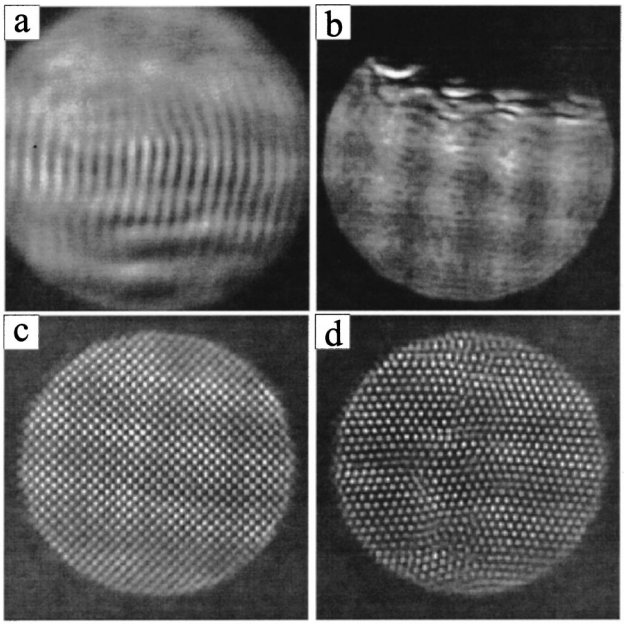

Fig. 6. Spatiotemporal instabilities (diffractive intensity patterns) in the adaptive system: (a) traveling waves originating from wave-front tilts on the order of 5λ, (b) traveling shock waves observed at the boundaries of the large-scale phase distortion area (heated Plexiglas plate), (c) square pattern, (d) hexagonal pattern. Wave-front control was based on iterative procedure (6) for (a) and (b) and (4) and (5) for (c) and (d); $\alpha = 0.3$ and $K = -8$ for (a), $\alpha = 0.8$ and $K = -10$ for (b), and $\alpha = 0.3$ and $K = -1$ for (c) and (d). Patterns (c) and (d) were obtained for the Gaussian spatial filter with characteristic bandwidths $q_{\text{cut}} = 1.2q_1$ for (c) and $q_{\text{cut}} = 1.5q_1$ for (d). In all cases $L = 4$ mm.

rector and a camera (diffractive feedback) and does not require either a reference wave or direct wave-front measurements. This adaptive system based on the diffractive-feedback principle is well suited as a high-resolution secondary wave-front control system. The diffractive-feedback system's insensitivity to large-scale wave-front aberrations leads to a reduction in cross talk between conventional and secondary adaptive systems and thus simplifies the entire adaptive system control algorithm.

The low adaptation speed of approximately 0.2 Hz—a major drawback of this adaptive system—is not the obligatory price one must always pay for high-resolution wave-front correction. The low adaptation rate is rather a result of hardware-related problems typical in proof-of-concept-type systems. The mismatch between the size and pixel geometries of the standard CCD camera and the LCTV panel resulted in time-consuming calculations related to scaling of the input (diffractive intensity) and output (controlling phase) images. This mismatch problem can be solved by using a customer-designed optically coupled phase SLM and photoarray (complementary metal-oxide semiconductor camera).

The second limitation is the operational rate of the high-resolution phase modulator. With the use of a LCTV panel, the maximum potential adaptive system speed cannot exceed 10–20 Hz. The alternatives to LCTV panels are fast LC phase SLM's and micro-electro-mechanical system (MEMS) mirrors. With the use of a commercially available LC phase SLM from Boulder Nonlinear Systems Inc. (spatial resolution of 128×128 or even 512×512 elements), adaptive system speed may potentially exceed 200–300 Hz.[14] Even higher speeds (up to 1 kHz and more) can be achieved when the new high-resolution MEMS mirrors soon become available.[15]

Phase corrector speed should be matched to adaptive system signal processing speed. This cannot be done by using conventional digital image processing architectures. One of the favorable features of the diffractive-feedback approach is the potential for parallel computations based on analog VLSI systems. Indeed, with the use of optical filtering, control algorithms (1) and (6) are well suited for analog VLSI implementation.[16] Integration of these existing technologies is a challenging task, with the reward being a new category of high-resolution, fast, and inexpensive adaptive optics technology.

APPENDIX A

Consider the spectral band $[q_A, q_B]$ and the corresponding spatial scale range of phase distortions that can be compensated by a diffractive-feedback adaptive system. For a simple low-pass spectral filter [$H(q) = 1$ for $q < q_1$ and $H(q) = 0$ otherwise], the adaptive system spectral coefficient for phase distortion suppression has the form[10]

$$T(q) = \frac{\Psi(q)}{\Phi(q)} = \frac{1}{1 - 2K \sin(q^2 L\lambda/4\pi)} \quad (0 < q < q_1), \tag{A1}$$

where $\Phi(q)$ and $\Psi(q)$ are spectral amplitudes of phase distortions for the input and output (corrected) waves and $K < 0$. The coefficient $T(q)$ characterizes efficiency of the diffractive-feedback adaptive system in compensating phase distortions. As seen from Eq. (A1), for $q \to 0$ (large-scale phase distortions) the spectral coefficient $T(q) \to 1$. This means that the adaptive system with diffractive feedback cannot compensate large-scale phase distortions.

To determine the adaptive system's spectral bandwidth, set the spectral coefficient T to 0.5 and find the corresponding spatial frequencies q_A and q_B from the condition $T(q_{A,B}) = 0.5$. Using Eq. (A1), we obtain

$$\sin(L\lambda q_{A,B}^2/4\pi) = 1/(2|K|),$$

$$q_A = [\pi^{-1} \arcsin(0.5|K|^{-1})]^{1/2} q_1,$$

$$q_B = q_1 - q_A. \tag{A2}$$

As seen from Eq. (A2), increasing the feedback gain coefficient $|K|$ leads to a corresponding increase of the adaptation spectral bandwidth. Knowledge of the spatial frequencies q_A and q_B allows estimation of the range of phase distortion spatial scales $r_l = 2\pi/q_A$ and $r_s = 2\pi/q_B$ that the adaptive system can compensate.

ACKNOWLEDGMENTS

I thank Gary Carhart for his assistance in developing the computer software used in the experiments, Rensheng Dou for calibrating the LCTV panel modulation characteristics, and J. C. Ricklin for technical and editorial com-

ments. This work was performed at the U.S. Army Research Laboratory's Intelligent Optics Laboratory in Adelphi, Maryland.

Mikhail A. Vorontsov can be reached at U.S. Army Research Laboratory, AMSRL-IS-C, 2800 Powder Mill Road, Adelphi, Maryland 20783, or by phone, 301-394-0214; fax, 301-394-0225; or e-mail, vorontsov@iol.arl.mil.

REFERENCES

1. J. W. Goodman, *Introduction to Fourier Optics* (McGraw-Hill, New York, 1968).
2. B. Y. Zeldovich, N. V. Pilipetsky, and V. V. Shkunov, *Principles of Phase Conjugation*, Vol. 42 of Springer Series in Optical Sciences (Springer-Verlag, Berlin, 1985); C. A. Primmerman, T. R. Price, R. A. Humphreys, B. G. Zollars, H. T. Barclay, and J. Herrmann, "Atmospheric-compensation experiments in strong-scintillation conditions," Appl. Opt. **34**, 2081–2088 (1995).
3. D. M. Pepper, C. J. Gaeta, and P. V. Mitchell, "Real-time holography, innovative adaptive optics, and compensated optical processors using spatial light modulators," in *Spatial Light Modulator Technology: Materials, Devices, and Applications*, U. Efron, ed. (Marcel Dekker, New York, 1995), pp. 585–654.
4. R. K. Tyson, *Principles of Adaptive Optics* (Academic, Boston, 1991); M. C. Roggemann and B. M. Welsh, *Imaging through Turbulence* (CRC Press, Boca Raton, Fla., 1996).
5. A. D. Fisher and C. Warde, "Technique for real-time high-resolution adaptive-phase compensation," Opt. Lett. **8**, 353–355 (1983).
6. M. A. Vorontsov, V. A. Katulin, and A. F. Naumov, "Wavefront control by an optical-feedback interferometer," Opt. Commun. **71**, 35–38 (1989); M. A. Vorontsov, M. E. Kirakosyan, and A. V. Larichev, "Correction of phase distortion in a nonlinear interferometer with an optical feedback loop," Sov. J. Quantum Electron. **21**, 105–108 (1991).
7. T. H. Barnes, T. Eiju, and K. Matsuda, "High resolution adaptive optics using an interference phase loop," Opt. Commun. **132**, 494–502 (1996).
8. W. J. Firth and M. A. Vorontsov, "Adaptive phase distortion suppression in a nonlinear system with feedback mirror," J. Mod. Opt. **40**, 1841–1846 (1993).
9. E. V. Degtiarev and M. A. Vorontsov, "Spatial filtering in nonlinear two-dimensional feedback systems: phase-distortion suppression," J. Opt. Soc. Am. B **12**, 1238–1248 (1995).
10. V. P. Sivokon and M. A. Vorontsov, "High-resolution adaptive phase distortion suppression based solely on intensity information," J. Opt. Soc. Am. A **15**, 234–247 (1998).
11. R. Dou and M. K. Giles, "Phase measurement and compensation of a wavefront using a twisted nematic liquid-crystal television," Appl. Opt. **35**, 3647–3652 (1996).
12. R. Dou and M. K. Giles, "Closed-loop adaptive-optics system with a liquid-crystal television as a phase retarder," Opt. Lett. **20**, 1583–1585 (1995).
13. R. Dou, M. A. Vorontsov, V. P. Sivokon, and M. K. Giles, "Iterative technique for high-resolution phase distortion compensation in adaptive interferometers," Opt. Eng. **36**, 3327–3335 (1997).
14. S. Serati, G. Sharp, R. Serati, D. McKnight, and J. Stookley, "128×128 analog liquid crystal spatial light modulator," in *Optical Pattern Recognition VI*, D. P. Casasent and T.-H. Chao, eds., Proc. SPIE **2490**, 55–59 (1995), and http://www.bnonlinear.com.
15. M. C. Roggeman, V. M. Bright, B. M. Welsh, S. R. Hick, P. C. Roberts, W. D. Cowan, and J. H. Comtois, "Use of micro-electro-mechanical deformable mirrors to control aberrations in optical systems: theoretical and experimental results," Opt. Eng. **36**, 1326–1338 (1997); M. C. Wu, "Micromachining for optical and opto-electronic systems," Proc. IEEE **85**, 1833 (1997).
16. A. G. Andreou and K. A. Boahen, "Translinear circuits in subthreshold MOS," Analog Integr. Circuits Signal Process. **9**, 141–166 (1996); C. A. Mead, "Neuromorphic electronic systems," Proc. IEEE **78**, 1629 (1990).